Charge and spin transport on graphene grain boundaries in a quantizing magnetic field

Madeleine Phillips and E. J. Mele

Phys. Rev. B **96**, 041403 — Published 5 July 2017

DOI: 10.1103/PhysRevB.96.041403

Charge and spin transport on graphene grain boundaries in a quantizing magnetic field

Madeleine Phillips and E. J. Mele*
Department of Physics and Astronomy,
University of Pennsylvania, Philadelphia PA 19104

(Dated: June 19, 2017)

We study charge and spin transport along grain boundaries in single layer graphene in the presence of a quantizing perpendicular magnetic field. Transport states in a grain boundary are produced by hybridization of Landau zero modes with interfacial states. In selected energy regimes quantum Hall edge states can be deflected either fully or partially into grain boundary states. The degree of edge state deflection is studied in the nonlocal conductance and in the shot noise. We also consider the possibility of grain boundaries as gate-switchable spin filters, a functionality enabled by counterpropagating transport channels laterally confined in the grain boundary.

PACS numbers: 72.80.Vp, 61.72.Mm, 73.43.Cd, 72.25.-b

Single layer graphene (SLG) grown by chemical vapor deposition (CVD) is often polycrystalline, with extended lattice defects forming the boundaries between misoriented grains. These grain boundaries (GBs) host laterally confined electronic states [1–4] and have attracted attention as possible linear transport channels (i.e. as atomically defined nanowires) [5]. In general, small group velocities along the tangent line and leakage into the conducting graphene bulk limit the practical use of GBs as wires; but in a quantizing magnetic field both these difficulties are avoided, and GBs can support transport channels that connect chiral exterior boundary states, short-circuiting the quantum Hall effect [6–9]. In this Rapid Communication we study this problem in the high field limit where the relativistic character of the Landau zero mode plays a crucial role in generating these GB transport states, and we use this insight to show how grain boundaries can be designed as configurable transport channels for charge and spin.

At low energies bulk single layer graphene hosts a valley degenerate massless relativistic electron gas which in a strong perpendicular magnetic field supports Landau zero modes. These are Landau levels that occur at the charge neutrality energy and are polarized on opposite sublattices in the two independent **k**-space valleys. Unlike the higher Landau levels (LLs), because of their sublattice polarization zeroth Landau levels (ZLLs) do not develop into dispersive edge modes by soft electrostatic confinement. Instead a ZLL can hybridize with a surface state at an atomically defined edge to form a *pair* of separately dispersive particle and hole branches [10]. This is the origin of the quantum Hall edge states in the first LL gap in graphene. A similar mechanism generates transport channels along graphene GBs where the ZLL becomes dispersive by hybridizing with low energy GB-confined states. The resulting states have a robust group velocity and, like the quantum Hall edge modes, are embedded in an incompressible electronic background. Here we point out that this mechanism for producing transport channels on GBs can apply to any extended defect in a "Dirac-like" bulk that hosts a low-energy defect band. The precise dispersion of the resulting branches will depend on the morphology of the defect band in zero field and provide a degree of structural control of the transport signatures.

The transport modes that develop on GBs by this mechanism are not chiral. Because the ZLL mixes with states living on the same defect in both valleys, one band corresponding to the interfacial mode must disperse away from $E = 0$ at the K point and then return to $E = 0$ on its way to the K' point. This results in interfacial bands that exist only in a bounded region in energy, so by tuning the chemical potential via a gate voltage, one can switch these GB-transport channels on and off. We discuss some unique applications enabled by this functionality: a current switch whose "on" and "off" energies are probed using the shot noise and a spin filter that generates spatially separated spin currents over a tunable energy range.

To illustrate these effects we present results for representative GB geometries: the 5-5-8 GB (Fig. 1a) a periodic line of octagons and pentagon pairs and the 5-7 GB (Fig. 1c) a line of pentagons and heptagons. The transport properties we obtain for these structures derive from their lattice connectivities and are described most clearly within a nearest neighbor tight binding Hamiltonian that ignores effects of small out of plane structural relaxations. The band structures for ribbon bicrystals partitioned by these GBs but without a magnetic field (Fig. 1b, d) show the closure of their projected bulk band gaps at critical values of the parallel momentum k_y and the appearance of surface/interface states within the gaps at low energy. For the case of the 5-5-8 GB the interfacial state is a symmetry protected flat band at $E = 0$ degenerate with the outer edge surface bands [3]. The 5-7 structure confines a narrow band of interfacial

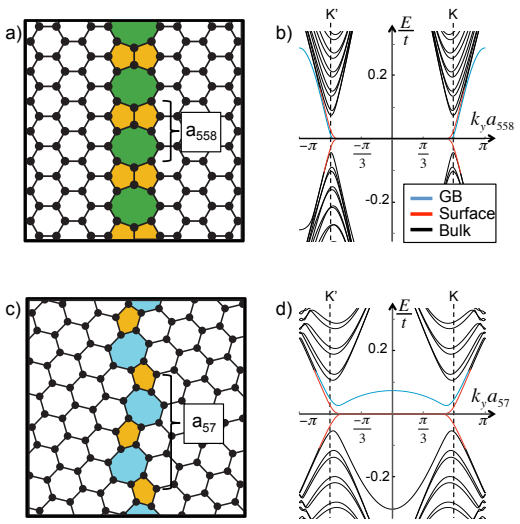

FIG. 1: Grain boundary lattices and their band structures in zero magnetic field. **a)** The 5-5-8 GB structure with period $a_{558} = 2a$, where a is the graphene lattice constant. **b)** Tight-binding band structure in units of the nearest neighbor tight binding parameter t for a 5-5-8 ribbon bicrystal. The flat band is triply degenerate with two surface states on opposite edges and one interfacial state. **c)** The 5-7 GB structure with period $a_{57} = \sqrt{13}a$. **d)** Band structure for a 5-7 ribbon bicrystal. Flat bands are doubly degenerate surface bands.

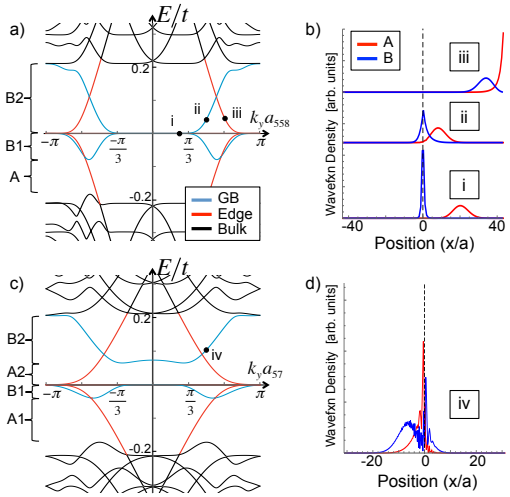

FIG. 2: Band structures for **a)** 5-5-8 and **c)** 5-7 GBs in a perpendicular magnetic field. Energy regions where GB transport states are accessible (inaccessible) are marked B (A). Flat bands near $k_y a = 0$ are triply (doubly) degenerate for 5-5-8 (5-7). The right panel shows charge densities projected onto the A (red) and B (blue) sublattices for energies/momenta marked in the band structures for **b)** the 5-5-8 and **d)** the 5-7 GB. State i in panel **b)** corresponds to one of three degenerate states at that k_y value. The overlap of surface/GB states with ZLL states shown in the right panel generates the dispersing bands in the left panel.

states away from the charge neutrality point as well as flat band surface states.

We focus on the pattern of edge and interfacial modes that occur when the bulk is gapped by a quantizing magnetic field. In the presence of a perpendicular field B we couple electronic motion to a vector potential $\vec{A} = Bx\,\hat{y}$ which retains periodicity along the GB and consider a field strength for which magnetic length, $\sqrt{\hbar/eB} \ll w$ where w is the ribbon width. Note that the bulk zeroth Landau level (ZLL) is polarized on opposite sublattices in each valley and is consequently pinned at $E = 0$. By constrast at momenta k_y where the ZLL wavefunction overlaps a grain boundary line it hybridizes with interfacial states to form a pair of composite dispersive bands (Fig. 2). In the Fig. 2 band structures, the outer edges modes (red) are chiral one-way modes with opposite velocities on opposite edges. This occurs because of the mismatch of the Chern number assigned to the first Landau gap ($\mathcal{C} = \pm 1$) and to the vacuum ($\mathcal{C} = 0$) which protects one chiral branch on each outer edge. By contrast across the interior grain boundary $\Delta\mathcal{C} = 0$ and interfacial modes with opposite velocities appear on the *same* boundary. These modes are the two branches of a one dimensional band with its "Fermi points" displaced in momenta. This can be contrasted with the situation for SLG snake states on interior boundaries, which can be produced in the quantum Hall regime either by reversal of the magnetic field or by sign reversal of the carrier type in a uniform field [11, 12], where across the interior boundary $\Delta\mathcal{C} = \pm 2$ protects pairs of co-propagating chiral modes on the domain wall. Backscattering is prohibited for snake states while for the GB states it is suppressed for smooth impurity potentials.

We consider a scenario where an outer quantum Hall edge state can be fully or partially deflected into the grain boundary. This type of deflection is generally very weak in an isolated graphene flake. Edge states and domain wall states contact only at isolated points of intersection. If the coupling between these channels were zero at these intersections then the momenta of the two degrees of freedom would be separately quantized in units $\propto 1/\mathcal{L}_c$ and $\propto 1/\mathcal{L}_w$ respectively where $\mathcal{L}_c$ is the flake perimeter and $\mathcal{L}_w$ is the length of the domain wall. Short range matrix elements connecting these two degrees of freedom scale $\propto 1/\sqrt{\mathcal{L}_c\mathcal{L}_w}$ and therefore couple these channels effectively only when the mixing scale greatly exceeds their energy separation, i.e. when $\sqrt{\mathcal{L}_w/\mathcal{L}_c} \ll 1$ which is typically not satisfied on a graphene flake. We have confirmed this kinematical obstruction in calculations on large flakes partitioned by grain boundaries where we find that edge modes and GB modes coexist as (nearly) independent degrees of freedom within the bulk Landau gaps. The former states circulate on the outer boundary and the latter states are observed as Fabry-Perot-like standing wave states laterally confined to the GB. The degree of decoupling is evident in the spatial distributions of the charge densities and velocity fields calculated for these

states [13]. States confined to the GB can be understood as the modes of a resonant cavity with a very high reflectivity at the contacts to the outer edges which does not admit useful switching of GB current pathways to or from an outer edge.

This kinematic decoupling can be avoided in an open system where the graphene is in contact with external particle reservoirs and its electronic states are lifetime broadened. We study transport in this regime using the scattering matrix formalism implemented in Kwant [14] to calculate the nonlocal conductances of multi-terminal Hall bars (Fig. 3). We consider a current biased system with current injected at electrode 4 and collected at 5 and obtain the nonlocal conductances by calculating the voltage states on all electrodes. Conductances calculated for a Hall bar without a grain boundary show quantized plateaus in the (spinless) Hall conductance at values $(2n+1)e^2/h$ (Fig. 3b). When the Hall bar is partitioned by a GB, the conductance measured between leads on the same side of the GB (G_{20}) continues to exhibit Hall plateaus, while the cross-GB Hall conductance (G_{XGB}) exhibits anomalous energy dependence (Fig. 3c, d). Considering only the bulk LL gap, in the A regions, G_{XGB} takes the Hall plateau values because transport occurs only in the chiral edge modes, but in the B regions the Hall plateaus break down due to cross-linking of the quantum Hall edges via the GB transport states [7]. When the chiral edge state is completely rerouted into the GB, $G_{XGB} \to 0$. These distinct spectral regimes (A and B) are the signature in the conductance of the gate-switchable nature of these devices. In the A regimes, the GB states are inaccessible, while in the B regimes current deflection is possible.

We can further quantify current deflection by studying the two terminal shot noise and Fano factor, which gives the ratio of the shot noise to its value in the uncorrelated (Poisson) limit. The Fano factor is $F = \sum_n T_n(1-T_n)/\sum_n T_n$, where T_n is the transmission probability in the $n-th$ channel [15]. Because the chiral edge states cannot backscatter, F captures only the partition noise at the junction between edge and interfacial states. Thus $F=0$ is the signature of perfect transmission from source to drain through an edge state (Fig. 4a, b). Conversely $F \sim 1$ occurs only in the strong deflection regime (Fig. 4c, d) where there are weak residual correlations between events that transmit discrete charges to the drain. Figure 4e, f shows that the Fano factor as a function of energy displays a sharp crossover from the edge state ($F=0$) to the interior channel ($F \sim 1$) regimes, underlining the possibility of turning source-to-drain transport "on" and "off" using a gate voltage.

These junctions can also be used as gate switchable spin filters. To study this we re-introduce the Zeeman coupling of the electron spin to the magnetic field. As shown in Figure 5 the spectrum is then spin split, and over a range of energy $\sim \Delta E_Z$ the edge mode can be

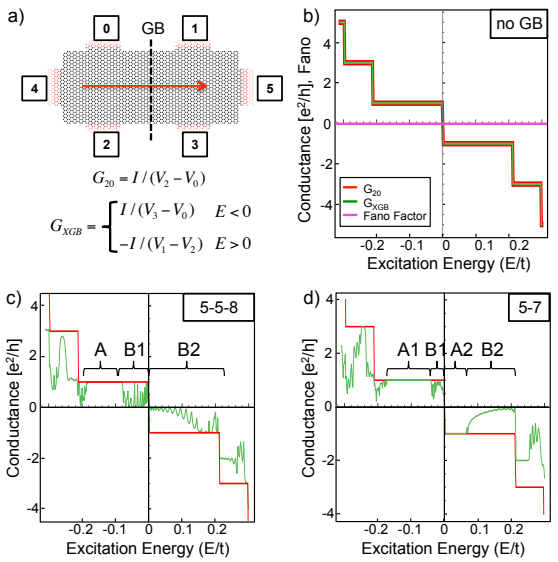

FIG. 3: **a)** Hall bar geometry for calculating conductances. Current I is injected at lead 4 and collected at lead 5. Voltages are calculated at each lead and used in expressions for non-local Hall conductance (G_{20}) and cross-GB conductance (G_{XGB}). **b-d)** G_{20} and G_{XGB} measured for Hall bars without a GB, partitioned by a 5-5-8 GB, and with a 5-7 GB. All panels show the quantization of the Hall conductance (G_{20}) on the left half of the Hall bar, and panels **c)** and **d)** show the breakdown of the Hall plateaus in G_{XGB} due to transport along the GB. A (B) spectral regions correspond to energies where GB transport is inaccessible (accessible). Panel **b)** includes the Fano factor ($F=0$) for the noiseless quantum Hall edge channels.

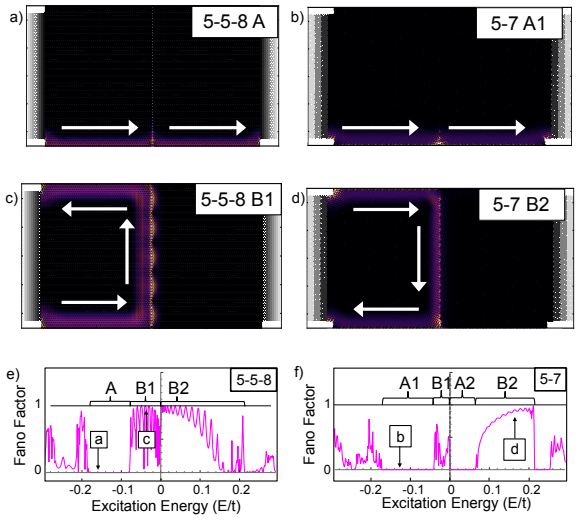

FIG. 4: **a-d)** Charge density maps of states matching an incoming plane wave with energy E from the left lead. All devices are $200a$ x $100a$ with lead width $80a$, where a is the graphene lattice constant. **e-f)** Fano factor as a function of energy for the 5-5-8 and 5-7 GBs, with sharp transitions from A to B regions suggesting switching functionality. Arrows indicate the energies of states a-d plotted in this figure.

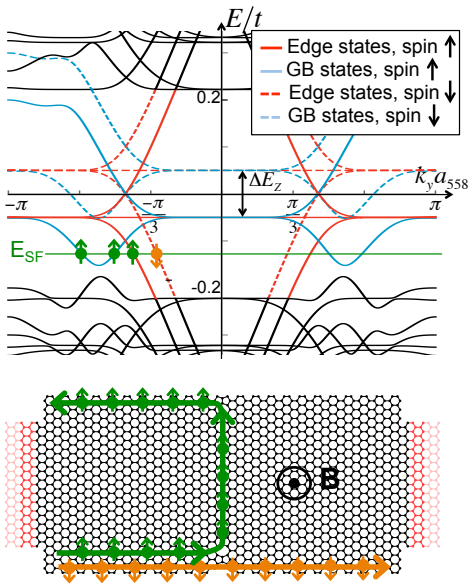

FIG. 5: **a)** Band structure for 5-5-8 GB ribbon with Zeeman splitting ΔE_Z. **b)** Schematic of the spin-filtering behavior of the GB at energy E_{SF}. Only spin-up current is deflected along GB.

deflected to the interior channel only for a single spin polarization. Note that this construction yields a spatial spin filter (i.e. it is a spin selective beam splitter) using the deflection into a GB current pathway only for a single spin polarization (Fig 5b). This can be compared with an earlier proposal for spin-selective transport at the edges of SLG in the quantum Hall regime [16, 18] where the Zeeman splitting of the Landau zero modes allows the particle and hole branches of its edge state spectrum to overlap in energy and produce helical edge modes. The helical modes are branches with opposite spin polarizations and velocities but residing on a common spatial boundary in contrast to the spatial separation of spin currents that occur for deflection into a GB.

These transport effects are seen most clearly in the first Landau gap. At higher energies edge states and grain boundary states also couple, but the spectra are congested as interfacial states begin to mix more with higher LL states.

Experimental demonstration of inter-edge charge transport along a graphene GB appears to be within reach of currently available materials. The fabrication of SLG containing 5-5-8 GBs has been demonstrated [5, 17] and the relevant energy ranges are accessible. For the pseudorelativistic spectrum in graphene the fundamental Landau gap between the zeroth and the first Landau levels is $\Delta_1 \sim 65\,\mathrm{K}\sqrt{B(T)}$, providing a sizeable energy window for observing these effects. The conditions for spin filtering are more restrictive since the bare Zeeman splitting $\Delta_z = g\mu_B B \sim 1.5\,\mathrm{K}\,B(T)$ $(g = 2)$ before accounting for an exchange enhancement of the g-factor [18, 19]. Note that strong interactions further complicate the situation in graphene in a strong perpendicular magnetic field since they gap the bulk even at charge neutrality [16, 18]. Although this has been attributed to an interaction-driven spin *unpolarized* state, experiments find that this phase undergoes a closing of the bulk gap marking a transition to a spin polarized state at only moderate value of the parallel magnetic field, $B_{\|} \sim 20\,T$ [16]. Transport measurements on the edge in this latter state show the signature of ballistic motion in helical channels within an energy window $g\mu_B B_{\mathrm{tot}}$. This high (tipped) field Zeeman-dominated phase is a promising setting for the spin filtering along a GB found in our calculations.

In summary, we demonstrate that transport states arise on extended defects in graphene when a low energy defect band hybridizes with the ZLL. We show results for two GB geometries, but any extended defect with an appropriate defect band could exhibit the same behavior. The non-chiral transport states that develop exist in finite energy regimes, opening the door for applications in gate-switchable charge and spin transport.

This work was supported by the Department of Energy under grant DE-FG02-84ER45118.

* Electronic address: mele@physics.upenn.edu

[1] A. Mesaros, S. Papanikolaou, C. F. J. Flipse, D. Sadri, J. Zaanen, Phys. Rev. B **82**, 205119 (2010).
[2] O. V. Yazyev and S. G. Louie, Phys. Rev. B **81**, 195420 (2010).
[3] M. Phillips, E. J. Mele, Phys. Rev. B **91**, 125404 (2015).
[4] A. Luican-Mayer, J. E. Barrios-Vargas, J. T. Falkenberg, G. Auts, A. W. Cummings, D. Soriano, G. Li, M. Brandbyge, O. V. Yazyev, S. Roche, 2D Mater. **3**, 031005 (2016).
[5] J. Lahiri, Y. Lin, P. Bozkurt, I. I. Oleynik, M. Batzill, Nature Nano. **5**, 326 (2010).
[6] A. Bergvall, J. M. Carlsson, T. Löfwander, Phys. Rev. B **91**, 245425 (2015).
[7] A. W. Cummings, A. Cresti, S. Roche, Phys. Rev. B **90**, 161401(R) (2014).
[8] V. Dal Lago and L. E. F. Foa Torres, J. Phys.: Condens. Matter **27**, 145303 (2015).
[9] F. Lafont, *et al.* Phys. Rev. B **90**, 115422 (2014).
[10] L. Brey and H.A. Fertig, Phys. Rev. B **73**, 195408 (2006).
[11] P. Rickhaus, P. Makk, M.-H. Liu, E. Tóvári, M. Weiss, R. Maurand, K. Richter, C. Schönenberger, Nat. Commun. **6**, 6470 (2015).
[12] Y. Liu, R. P. Tiwari, M. Brada, C. Bruder, F. V. Kusmartsev, E. J. Mele, Phys. Rev. B **92**, 235438 (2015).
[13] See Supplemental Material at [URL will be inserted by publisher] for isolated flake calculations, further details about Kwant calculations, and supporting data describing a third grain boundary.
[14] C. W. Groth, M. Wimmer, A. R. Akhmerov, X. Waintal, *Kwant: a software package for quantum transport,* New J. Phys. **16**, 063065 (2014).

[15] Ya.M. Blanter, M. Büttiker, Phys. Reports **336**, 1-166 (2000).
[16] A.F. Young, *et al.* Nature **505**, 528 (2014).
[17] J.-H. Chen, G. Autès, N. Alem, F. Gargiulo, A. Gautam, M. Linck, C. Kisielowski, O. V. Yazyev, S. G. Louie, A. Zettl, Phys. Rev. B **89**, 121407(R) (2014).
[18] D.A. Abanin, P.A. Lee and L.S. Levitov, Physical Review Letters **96**, 176803 (2006)
[19] A.V. Volkov, A. A. Shylau, I. V. Zozoulenko, Phys. Rev. B **86**, 155440 (2012).